### Title

Atomistic simulations of thermal conductivity in GeTe nanowires




### Journal

Journal of Physics D, 53(5)

### ISSN

0022-3727



### Authors

Bosoni, E

Campi, D

Donadio, D

et al.



### Publication Date

2020-01-30

### DOI

10.1088/1361-6463/ab5478

Peer reviewed

# Atomistic Simulations of Thermal Conductivity in GeTe Nanowires

**E Bosoni[1]‡, D Campi[1], D Donadio[2], G C Sosso[3], J Behler[4] and M Bernasconi[1]**

[1]Dipartimento di Scienza dei Materiali, Università di Milano-Bicocca, Via R. Cozzi 55, I-20125 Milano, Italy
[2]Department of Chemistry, University of California Davis, One Shields Avenue, Davis, California 95616, U.S.A.
[3]Department of Chemistry and Centre for Scientific Computing, University of Warwick, Gibbet Hill Road, Coventry CV4 7AL, UK.
[4]Universität Göttingen, Institut für Physikalische Chemie, Theoretische Chemie, Tammannstr. 6, 37077 Göttingen, Germany.

E-mail: marco.bernasconi@unimib.it

**Abstract.** The thermal conductivity of GeTe crystalline nanowires has been computed by means on non-equilibrium molecular dynamics simulations employing a machine learning interatomic potential. This material is of interest for application in phase change non-volatile memories. The resulting lattice thermal conductivity of an ultrathin nanowire (7.3 nm diameter) of 1.57 W/mK is sizably lower than the corresponding bulk value of 3.15 W/mK obtained within the same framework. The analysis of the phonon dispersion relations and lifetimes reveals that the lower thermal conductivity in the nanowire is mostly due to a reduction in the phonon group velocities. We further predict the presence of a minimum in the lattice thermal conductivity for thicker nanowires.

*Keywords*: Phase Change Materials, Nanowires, Neural Networks, Thermal transport, Molecular Dynamics Simulations

Submitted to: *J. Phys. D: Appl. Phys.*

‡ Present address: School of Physics and CRANN, Trinity College Dublin.

## 1. Introduction

Phase Change Memories (PCMs) are leading contender for the development of storage class memories which combine non-volatility with access times of the order of 10-100 ns which are close to those of DRAM technologies [1].

PCMs rely on a fast and reversible crystalline-to-amorphous transformation of a chalcogenide alloy induced by Joule heating [2, 3, 4, 5, 6, 7]. Read out of the memory consists of the measurement of the resistance at low bias which is suitable to discriminate the two phases of the active material displaying a difference in electrical resistivity of about three orders of magnitude. Joule heating at higher voltage induces either the amorphization of the crystal (reset process) via crystal melting, or the recrystallization of the amorphous (set process).

A unique portfolio of features makes $Ge_2Sb_2Te_5$ (GST) the material of choice for PCM application, but other chalcogenides including doped GeTe [8] and $Sb_2Te_3$ [9] are also under scrutiny. Phase change memories developed by Intel and Micron entered the market in 2017 as storage class memories with the commercial name of Optane featuring GST cells in a 3D crossbar array architecture [10].

Further development of storage class memory based on PCMs would benefit from an overall reduction of power consumption for the set/reset processes. An attractive option in this respect involves the use of nanowires (NWs) [11, 12] that keep a high crystallinity down to very low scale. Many studies have been devoted to the synthesis and electrical characterization of chalcogenides NWs made of different GeSbTe alloys [11, 13, 14, 15, 16, 17], GeSb [18], $Sb_2Te_3$ [19, 20, 21], GeTe [12, 17, 22, 23, 24, 25, 26, 27, 28]. Ultrathin InSbTe NWs with diameter below 15 nm have also been synthesized by metal organic chemical vapor deposition methods [29].

In addition to the size reduction, other advantages of NWs with respect to bulk materials have been reported, most notably a reduction of the resistance drift in the reset state and a reduction of the programming current. In fact, while the crystal is stable, the metastable amorphous phase is subject to aging which leads to an increase in the electrical resistivity with time. This phenomenon, called drift [30, 31, 32], is detrimental for the operation of PCMs and it has been shown to be substantially reduced in NWs with respect to the bulk [33, 34]. On the other hand, the reduction of the programming current in NWs is ascribed to several concurrent effects, namely heat and electric current confinements due the reduced sectional area [12] and to a lower melting temperature for the reset operation [25, 34, 35].

Thermal transport is a key property for the confinement of heat which is strongly affected by the reduction of dimensionality [36, 37]. Heat is physically confined along the radial direction of the NW, but a reduction of the thermal conductivity with respect to the bulk is also expected along the growth direction of the NW [38]. For sufficiently large NWs, scattering of phonons by the free surfaces can account for the reduced thermal conductivity as implemented in different phenomenological models [39]. However, changes in the phonon dispersion relations and phonon-phonon scattering with respect to the bulk have to be properly taken into account to describe thermal conductivity in thin NWs [39]. These effects are responsible, for instance, for an increase of the lattice thermal conductivity upon decreasing the diameter in ultrathin (1-5 nm) Si nanowires as reported by atomistic simulations [40, 41].

In this work, we make use of non-equilibrium molecular dynamics simulations (MD) to predict the lattice thermal conductivity of NWs of the phase change compound GeTe. We focus on this material because of the availability of a reliable interatomic potential for large scale simulations [42].

At normal conditions GeTe crystallizes in the $\alpha$ phase with trigonal geometry (space group R3m) [43]. This phase can be viewed as a distorted rock-salt geometry with an elongation of the cube diagonal along the [111] direction and an off-center displacement of the inner Te atom along the [111] direction giving rise to a 3+3 coordination of Ge with three short and three long bonds (2.84 and 3.17 Å). The structure can be also seen as an arrangement of GeTe bilayers along the $c$ direction of the hexagonal cell with shorter intrabilayer bonds and longer interbilayers bonds. The $\alpha$-phase transforms into the a cubic phase ($\beta$-GeTe, space group $Fm\bar{3}m$) above the ferroelectric critical temperature of 705 K [44]. In the cubic phase, the alternation of long and short bonds survives in a disordered manner along all equivalent $<111>$ directions as shown by extended x-ray absorption fine structure and x-ray total diffraction measurements [45, 46].

Experimental data on thermal conductivity are available only for relatively large NWs of $\alpha$-GeTe with diameter in the range 80-160 nm, probably not of interest for PCM applications due to their size [47]. For these NWs a total (electronic plus lattice) thermal conductivity of 1.44 W/mK was reported [47]. This value is sizably lower than the total thermal conductivity of $3.8 \pm 0.53$ W/mK measured for bulk crystalline GeTe [48].

To shed light of the origin of the reduction in the

thermal conductivity in NW, we here study ultrathin NWs (7.3 nm in diameter) of $\alpha$-GeTe.

After the brief outline of the computational methods (Section 2) and a discussion on the choice of the NWs geometry (Section 3.1) we discuss in Section 3.2 the results on the lattice thermal conductivity of the GeTe NW with 7.3 nm diameter and the origin of the reduced thermal conductivity with respect of the bulk. On the basis of this analysis, we then attempt to estimate the lattice thermal conductivity of NWs with different diameters. Finally, Section 4 is devoted to the conclusions.

## 2. Computational Details

Molecular dynamics (MD) simulations have been performed by using the Neural Network (NN) interatomic potential developed in [34, 42]. The NN interatomic potential of GeTe was originally obtained in [42] by fitting a database of total energies obtained within Density Functional Thoery (DFT) by means of the method introduced by Behler and Parrinello [49]. The database consists of the total energies of about 30000 configurations of 64-, 96-, and 216-atom supercells computed within DFT by employing the Perdew-Burke-Ernzerhof (PBE) exchange and correlation functional [50] and norm conserving pseudopotentials. The NN potential displays an accuracy close to that of the underlying DFT-PBE framework whose reliability in describing structural and dynamical properties of GeTe and other phase change materials has been validated in several previous works [51, 52, 53, 54]. The transferability of the NN potential was validated in previous works on bulk liquid, amorphous, and crystalline GeTe [42, 55, 56, 57, 58].

In order to deal with NWs, a new version of the NN potential was generated in [34] by enlarging the training set with about 5000 new configurations of crystalline and amorphous GeTe in a slab geometry (128-atom supercell) and about 7000 new configurations of crystalline, amorphous and liquid GeTe in a NW geometry (120- and 256-atoms cells).

To compute the thermal conductivity, we used the reverse non-equilibrium molecular dynamics (RNEMD) scheme proposed by Müller-Plathe [59]. In this method, one sets up a stationary heat flux density $J$ between a source and a sink at the two edges of the simulation cell, which gives rise to a stationary temperature gradient $dT/dz$ from which the thermal conductivity is computed by Fourier's law as $\kappa = -J/(dT/dz)$.

The RNEMD simulations were performed with the NN code RuNNer [60] by using the DL_POLY code [61] as molecular dynamics driver with a time step of 2 fs.

The RNEMD technique with the NN interatomic potential was used in our previous work [56] to calculate the lattice thermal conductivity of amorphous GeTe ($\kappa$ = 0.26 W/mK) which was in excellent agreement with experimenal data (0.23 $\pm$ 0.04 W/mK from [48]) and very close to the previous result of 0.27 $\pm$ 0.05 W/mK obtained from equilibrium MD and the use of the Green-Kubo formula [55]. All the values of the thermal conductivity computed here or referred to from literature correspond to 300 K.

The RNEMD technique with the NN interatomic potential was also used to compute the thermal conductivity of crystalline $\alpha$-GeTe which yielded $\kappa_x$ = $\kappa_x$ = 3.15 $\pm$ 0.2 W/mK and $\kappa_z$ = 3.23 $\pm$ 0.1 W/mK [56], where $x$, $y$ and $z$ refer to the components of the conductivity tensor along the three cartesian directions with $z$ along the $c$ axis of $\alpha$-GeTe in the hexagonal notation.

The new version of the NN potential [34], suitable to be used for NWs, yields the same lattice thermal conductivity for crystalline and amorphous GeTe (within the error bar given above) of the former version discussed in [42].

The average thermal conductivity suitable to describe a polycrystalline material is obtained as $\kappa_{av}$=$\frac{2}{3}\kappa_x$ + $\frac{1}{3}\kappa_z$= 3.18 W/mK, provided that phonon scattering from grain boundaries could be neglected. We remark that this theoretical value of the bulk thermal conductivity of $\alpha$-GeTe is an upper bound as it refers to a perfect crystal with no defects, while a large concentration of Ge vacancies is actually present in the real material conferring a p-type degenerate character [62]. In our previous work [63], we have shown that $\kappa_{av}$ of $\alpha$-GeTe can decrease from 3.2 W/mK for the perfect crystal to 2.7 W/mK for the vacancy content of 0.2 atom$\%$ measured for instance in [62]. The phonon scattering due to vacancies brings the theoretical value close to the experimental lattice thermal conductivity of 2.35 $\pm$ 0.53 W/mK measured in [48]. The results in [63] were obtained on the basis of harmonic and anharmonic force constants computed within the Density Functional Perturbation Theory (DFPT) [64] in the Local Density Approximation and the solution of the Boltzmann phonon transport equation.

Note that the DFPT calculations of Ref. [63] yield an anisotropic thermal conductivity for ideal GeTe (no defects) with $\kappa_x$ = 3.62 W/mK and $\kappa_z$ = 2.37 W/mK, while the anisotropy predicted by RNEMD simulations with the NN potential is actually smaller than the error bar on the thermal conductivity itself as reported above. This has to be ascribed to a limitation of the NN potential. The phonon dispersion relation of $\alpha$-GeTe computed with the new NN potential are compared with DFT results in Figure 1. The DFT data refer to a hole-doped system with hole concentration of 8 $\cdot$ $10^{19}$ holes/cm$^3$ as discussed in our previous work [63]. The presence of holes makes the system metallic and it allow neglecting the non-analytic part of the dynamical matrix due to long-range Coulomb interactions responsible for LO-TO splittings. These splitting are absent in the NN results as well due to the short range character of this interatomic potential. NN potentials can usually provide a much better agreement with DFT phonons than that shown in Figure 1 once the

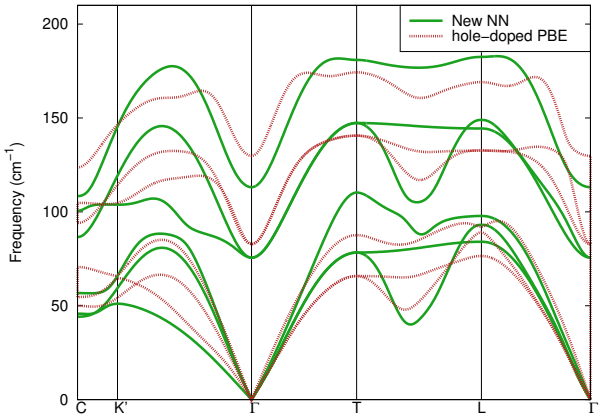


**Figure 1.** (Color online) Phonon dispersion relations of $\alpha$-GeTe along high symmetry directions of the Brillouin Zone computed with the new NN potential [34] and by DFT with the PBE functional for a hole-doped system as reported in [63] which we refer to for further details. The path in the BZ is the same reported in Refs. [63] and [56]. Point K$'$ is (-0.37165,-0.7567,-0.37165), and point C is (-0.5, 1.0, -0.5); these points were erroneously labelled K and X in the phonon dispersions of Refs.[63] and [56], but they do not actually correspond to the point K, X shown on the figure of the BZ in Ref. [56].

potential is specifically devised for this purpose with limited transferability for the simulations of other properties [65]. In our case, we note that the NN potential was devised to reproduce structural and dynamics properties of liquid, amorphous and crystalline GeTe in the bulk and in reduced dimensions. This wide applicability of the NN potential came at the expense of a lower quality, albeit acceptable, of the NN phonons for the crystalline phase.

## 3. Results

### *3.1. Modeling of GeTe Nanowires*

In a previous work [34], we built a model of a GeTe nanowire with a diameter of about 9 nm. The [220] growth axis (in the hexagonal notation with the redundant index omitted) was chosen according to the geometry of the NWs synthesized experimentally by different means [22, 23, 24]. In our NW model the $(1\bar{1}2)$ surfaces and the (001) surfaces terminated by Te were exposed. These surfaces were chosen on the basis of their thermal stability as described in our previous work [34].

For the calculation of the thermal conductivity by RNEMD, we have built a similar, thinner NW with a diameter of 7.3 nm and with the same exposed surfaces. As it occurs for the larger NW, this latter model undergoes a reconstruction with the removal of net electric dipoles and with the formation of twin boundaries. The primitive cell of the NW is 16.93 Å long (along the growth direction) and it contains 2164 atoms (1036 Ge and 1128 Te). In the inner part of the NW, the reconstruction leads to the formation of a misoriented domain of the trigonal phase (448 atoms

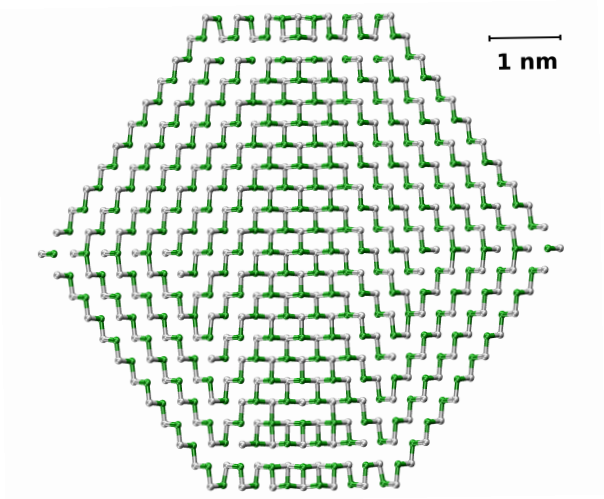


(a)

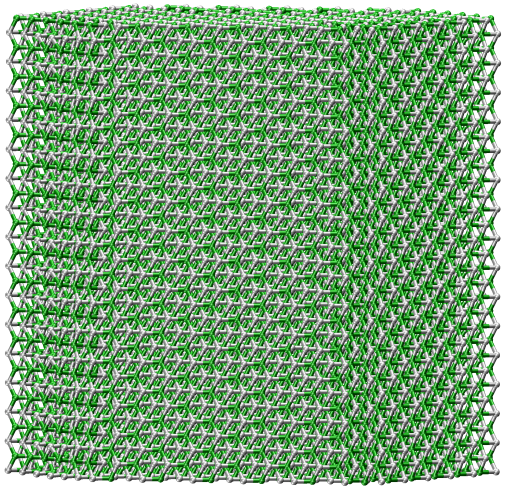

(b)

**Figure 2.** (Color online) (a) Cross section and (b) side view of the GeTe NW used in the simulations. The NW has a hexagonal section with a diameter of about 7.3 nm. Only four unit cells along the growth direction are shown, while the model used in the RNEMD simulation consists of 23 unit cells (49772 atoms).

large out of 2164 ones) with the $c$ axis forming an angle of 33.8% respect to the growth direction, as it occurs in the larger model of [34]. A cross section and side views of the NW are shown in Figure 2. A file with the Cartesian atomic coordinates and cell edges of the 2164-atom unit cell of the crystalline NW is provided in the supplementary material.

### *3.2. Thermal conductivity*

A crucial issue in RNEMD simulations is the choice of length of the simulation cell that must be longer than the phonons mean free path to properly include the

relevant scattering processes. A previous DFT study of thermal conductivity of bulk $\alpha$-GeTe shows that all phonons significantly contributing to heat transport have a mean free path shorter than 40 nm (see Figure 3 in [63]) which is consistent with the results of [56] showing that a cell of about 50 nm is sufficiently long to get a converged thermal conductivity in RNEMD simulations of crystalline GeTe. The cumulative thermal conductivity of bulk $\alpha$-GeTe as a function of phonon mean free path is reported in Figure 3. These results, obtained from the DFT data of Ref. [63], show that phonons with mean free path longer than 40 nm contribute very little to the lattice thermal conductivity. Since the phonon mean free path is expected to be shorter in the NWs than in the bulk, we used here a simulation cell of 40 nm along the growth direction of the NW (7.3 nm wide) which contains a total number 49772 atoms.

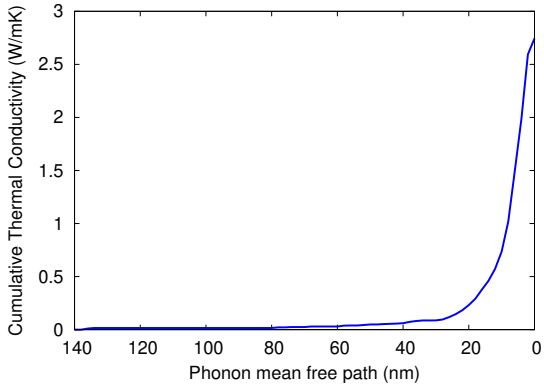


**Figure 3.** Cumulative average thermal conductivity $\kappa(L)$ as a function of mean free path $L$ of bulk $\alpha$-GeTe. The function $\kappa(L)$ is the thermal conductivity due to all phonons with mean free path longer than $L$. The data are obtained from the DFT results of Ref. [63] which refer to the solution of the Boltzmann equation within the Single Mode Relaxation Time Approximation.

In the RNEMD simulations, we exchanged the kinetic energy of the hottest atom in the cold source with the kinetic energy of the coldest atom in the hot source every 75 steps which lead to a stationary heat flux $q$ after 1.2 ns as shown in the upper panel of Figure 4. The hot and cold sources are placed at the edges of the cell along the $z$-direction, they consists of a slice of mobile atoms 5 Å thick along $z$ neighboring a region of fixed atoms, which decouple the two sources in the presence of periodic boundary conditions. The stationary profile of the temperature along the NW, averaged over 200 ps after equilibration, is shown in the lower panel of Figure 4.

The resulting lattice thermal conductivity of the NW is $\kappa$=1.57$\pm$0.04 W/mK as obtained from the temperature gradient and the value of the heat flux density $J$=$q$/$A$, where the section of the NW is $A$ = 3281 Å$^2$.

Since the growth direction lies in the xy plane of bulk $\alpha$-GeTe (in the hexagonal notation with the $c$ axis along z), the value of $\kappa$ for the NW has to be compared with the value $\kappa_x$ = 3.15 $\pm$ 0.20 W/mK for bulk $\alpha$-GeTe obtained with the NN potential and RNEMD in [56].

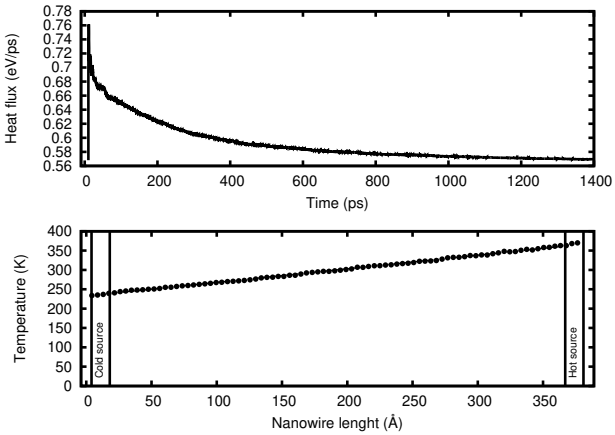


**Figure 4.** (Upper panel) Heat flux as a function of time in RNEMD of the NW with a diameter of 7.3 nm. (Lower panel) Temperature profile along the simulation cell in stationary conditions.

We thus reproduce a substantial reduction of the thermal conductivity in the NW with respect the bulk as observed experimentally for large NWs in [47]. However, a direct comparison with the experimental data is not possible because of several reasons: our NW is much thinner than in experiments (7.3 nm versus 80-160 nm), electronic contribution to the thermal conductivity is present in the experimental data while we compute only the lattice contribution, we considered an ideal crystalline NW with no Ge vacancies while a large concentration of vacancies is expected in real materials in both bulk and NWs.

Therefore, we restricted ourselves to a comparison between theoretical results for the NW and the bulk in order to assess the origin of the reduction of the lattice thermal conductivity in the NWs. To this end, we used the following expression for the lattice thermal conductivity of a crystal along a direction $\alpha$ given by the solution of the Boltzmann Transport Equation (BTE) in the Single Mode Relaxation Time Approximation (SMA):

$$\kappa_\alpha = \frac{1}{N_0 V} \sum_{j\mathbf{q}} \hbar\omega(\mathbf{q},j) v_\alpha^2(\mathbf{q},j) \frac{\partial f_B(\omega(\mathbf{q},j))}{\partial T} \tau(\mathbf{q},j) \quad (1)$$

where the sum runs over the band index $j$ and $N_0$ points $\mathbf{q}$ in the Brillouin Zone (BZ), $v_\alpha(\mathbf{q},j)$ is the group velocity along the direction $\alpha$ of the $(\mathbf{q},j)$ phonon with frequency $\omega(\mathbf{q},j)$. $f_B$ is the Bose-Einstein distribution function, $V$ is the unit cell volume, and $\tau(\mathbf{q},j)$ is the phonon lifetime. The same expression holds for a NW once the one dimensional BZ is considered and $V$=$A \cdot L$ where $L$ is the length and $A$ the cross sectional area of the NW. The applicability of the SMA is discussed in [63] where it is shown that for $\alpha$-GeTe this approximation underestimates the lattice thermal conductivity by about 15 % with respect to the full solution of the BTE.

The reduction in the thermal conductivity in the NW might arise from a change in the phonon lifetimes, in the

group velocities and/or in the phonon density of states. All these three quantities entering in (1) can be computed for the bulk, but the calculation of the phonon lifetime in the NW is too computationally demanding. Therefore, we tried to use (1) for the NW by making use of the bulk phonon lifetimes in order to assess the effect of the change in the group velocities and density of states on the thermal conductivity. To this end, we first introduced averages over bands and $\mathbf{q}$ points of the group velocities and phonon lifetime as

$$v_\alpha^2(\omega) = \frac{\sum_{j\mathbf{q}} v_\alpha^2(\mathbf{q},j)\delta(\omega-\omega(\mathbf{q},j))}{\sum_{j\mathbf{q}}\delta(\omega-\omega(\mathbf{q},j))}, \quad (2)$$

$$\tau(\omega) = \frac{\sum_{j\mathbf{q}} \tau(\mathbf{q},j)\delta(\omega-\omega(\mathbf{q},j))}{\sum_{j\mathbf{q}}\delta(\omega-\omega(\mathbf{q},j))}. \quad (3)$$

Then, by introducing the phonon Density of States (DoS) $D(\omega)$ (states/cm$^{-1}$/Å$^3$) we approximate (1) as an integral over frequency only as

$$\kappa_\alpha = \int_0^{\bar{\omega}} d\omega\, \hbar\omega D(\omega) v_\alpha^2(\omega) \frac{\partial f_B(\omega)}{\partial T}\tau(\omega) \quad (4)$$

where $\bar{\omega}$ is the highest phonon frequency of the material. An isotropic average for bulk materials can be obtained simply as $\kappa_{av} = (\kappa_x + \kappa_y + \kappa_z)/3$, resulting in:

$$\kappa_{av} = \frac{1}{3}\int_0^{\bar{\omega}} d\omega\, \hbar\omega D(\omega) v^2(\omega) \frac{\partial f_B(\omega)}{\partial T}\tau(\omega) \quad (5)$$

where

$$v^2(\omega) = v_x^2(\omega) + v_y^2(\omega) + v_z^2(\omega) \quad (6)$$

For $\alpha$-GeTe, $z$ refers to the $c$ axis of the hexagonal cell and the directions $x$ and $y$ are equivalent.

We checked the validity of this approach by comparing the results of (4) and (1) for bulk GeTe by using the DFPT data reported in our previous work [63]. It turns out that (4) overestimates the SMA result of (1) by about 8% which is an error sufficiently small for our purposes.

We then computed all quantities entering in (5) with the NN potential for bulk GeTe. $D(\omega)$, $v(\omega)$ and $\tau(\omega)$ are reported in Figure 5. Phonon lifetimes have been computed from third order anharmonic force constants obtained by finite differences in a 1152-atom supercell, by considering only $\Gamma$-point phonons. The explicit expression of the phonon lifetime in terms on anharmonic force constants is given for instance by Eq. (B2) in [66]. $D(\omega)$ and $v^2(\omega)$ are averages over a 40x40x40 mesh of $\mathbf{q}$ points in the BZ of the primitive cell (two atoms). Since phonons with frequency below 8 cm$^{-1}$ are not present at the $\Gamma$-point of the 1152-atom supercell, their lifetime was taken equal to 30 ps which is the average lifetime of phonons at about 10 cm$^{-1}$. The resulting cumulative thermal conductivity from (5) is shown in Figure 5d. The final $\kappa_{av}$ of 3.53 W/mK is comparable, albeit higher, to the RNEMD value of 3.18 W/mK discussed above.

We then used Eq. (4) to investigate the role of the change in the phonon density of states and of the group

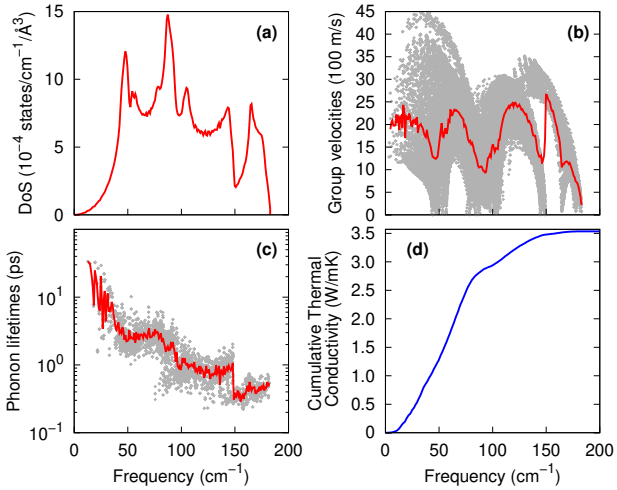


**Figure 5.** (Color online) a) Phonon density of state, b) distribution of phonon group velocities, and c) distribution of phonon lifetimes for crystalline bulk GeTe computed with the NN potential. The continuous lines in panels b) and c) are the averages $v(\omega)$ and $\tau(\omega)$ defined in (6) and (3). d) Cumulative average thermal conductivity ($\kappa_{av}$) from (5).

velocities in the reduction of the thermal conductivity in the NW. We computed the group velocities of the NW by averaging in (2) over eight $\mathbf{q}$ points in the one dimensional BZ, while the DoS has been computed on a mesh of 40 $\mathbf{q}$ points. The results are compared in Figure 6 with the bulk values for the DoS and $|v_\alpha(\omega)|$ with $\alpha$ along the growth direction of the NW ([220]). Note that in an isotropic material, $v_\alpha^2(\omega)$ along a generic direction $\alpha$, averaged over the BZ, is 1/3 of the average of $v^2(\omega)$ defined in (6), hence the factor of about $1/\sqrt{3}$ between the group velocities in the bulk in Figure 5 and Figure 6. The group velocities are drastically reduced in the NW in the frequency range 50-140 cm$^{-1}$, while they are comparable or even higher than in the bulk for frequencies below 25 cm$^{-1}$. Overall the distribution of heat carriers is shifted toward lower frequencies in NW with respect to the bulk.

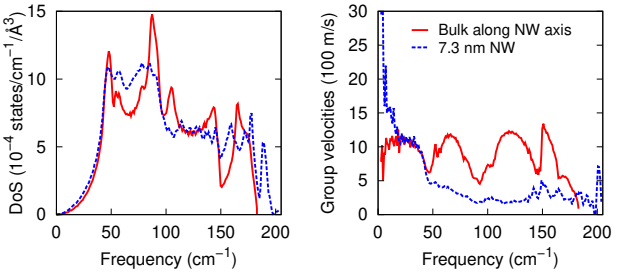


**Figure 6.** (Color online) (Left panel) Phonon density of states of the NW and of the bulk. (Right panel) Phonon group velocities in the NW (diameter of 7.3 nm) compared with the group velocities in the bulk along the direction equivalent to the NW axis.

By plugging into (4) the DoS of the NW and by keeping $\tau(\omega)$ and $v_\alpha^2(\omega)$ of the bulk with $\alpha$ along the growth direction of the NW, we obtain $\kappa$=3.73 W/mK.

This result shows that the modification in the DoS is not sufficient to explain the reduced thermal conductivity in the NW. On the contrary, by plugging in (4) both the DoS and the group velocities of the NW and by still keeping the phonon lifetime $\tau(\omega)$ of the bulk, we obtain $\kappa$=1.87 W/mK which is only slightly higher than the RNEMD value of 1.57 W/mK for the NW, even though changes in lifetimes are not considered. Therefore, although we also expect a change of the phonon lifetime in the NW with respect to the bulk, we can conclude that most of the reduction of the thermal conductivity in our NW stems from a reduction of the phonon group velocities.

On the basis of this analysis, we attempted to estimate the thermal conductivity of NWs of different diameters by using (4). To this end, we built two other NWs of diameter 6.5 nm and 11.6 nm as shown in Figure 7. Moreover, we also considered the 9.0 nm NW discussed in our previous work [34]. For these three NWs we computed the DoS and the group velocities. The distributions of the group velocities for all the NWs are compared in the left panel of Figure 8. The dispersion relations of phonons at low frequencies along the growth direction are shown in the right panel of Figure 8 for two representative NW diameters. The product $D(\omega) \cdot v_\alpha^2(\omega)$ is compared for different NWs in the left panel of Figure 9. Then, we estimated the lattice thermal conductivity of the NWs by plugging in (4) the function $D(\omega) \cdot v_\alpha^2(\omega)$ for the different NWs by still keeping the phonon lifetimes $\tau(\omega)$ of the bulk, as we reported above for the 7.3 nm wide NW. The cumulative thermal conductivity of the NW is shown in the right panel of Figure 9 while the results for $\kappa$ are collected in Table 1.

**Table 1.** Thermal conductivity as a function of the NW diameter computed from (4) with DoS and group velocities of the NW and phonon lifetimes of the bulk (see text).

| Diameter (nm) | $\kappa$ (W/mK) |
|---|---|
| 6.5 | 2.11 |
| 7.3 | 1.87 |
| 9.0 | 1.58 |
| 11.6 | 1.33 |

We observed that the thermal conductivity increases by decreasing the diameter of the NW. This would be surprising if one assumes that the phonon mean free path in nanostructure is limited by the characteristic dimension of the system, i.e. the diameter for nanowires, according to the Casimir limit. However, this is a general behavior that stems from the onset of anomalous transport in low-dimensional systems, as predicted for non linear models [67] and observed in carbon nanotubes, graphene and even SiGe nanowires [68, 69, 70]. In these systems the thermal conductivity either diverges with length or converges only for macroscopic lengths. This trend is enhanced at small diameter/thickness, as the material becomes more low-dimensional [71]. For example, for crystalline silicon nanowires with diameter smaller than 5 nm it was observed that, in the absence of surface defects, the thinner the wire the higher the thermal conductivity [40, 41].

In the case of GeTe, this behavior can be explained by inspection of Figures 8 and 9 as follows. As discussed above, the origin of most of the reduction of the thermal conductivity in the NW (7.3 nm wide) with respect to the bulk is due to the lower group velocities in the NW for frequency above 50 $cm^{-1}$ which involves acoustic branches at the BZ boundary and the optical phonons (see Figure 1). This is partially compensated by higher group velocities in the NW at frequency lower than 25 $cm^{-1}$. In the range 25-50 $cm^{-1}$ the group velocities are nearly equal to those of the bulk for the NW of 7.3 nm, while they are lower (higher) than in the bulk for diameters lower (larger) than 7.3 nm. This effect leads to an increase of the thermal conductivity by decreasing the section of the NW in the range 6.5-11.6 nm investigated here. In the case of silicon crystalline nanowires as well, one observes an increase in the group velocity of the longitudinal acoustic branch. Whether this is sufficient to explain the increase of the thermal conductivity by reducing the diameter in ultrathin Si nanowires, it remains to be seen.

## 4. Conclusions

In summary, we have computed the lattice thermal conductivity of an ultrathin crystalline nanowire of the phase change compound GeTe. The nanowire model has a hexagonal-like section with a diameter of about 7.3 nm and the growth axis along the [220] direction of trigonal $\alpha$-GeTe (in the hexagonal notation with the redundant index omitted). The thermal conductivity has been computed by means of the non-equilibrium molecular dynamics method introduced in [59] using an interatomic potential generated with a Neural Network method in previous works [34, 42]. The resulting lattice thermal conductivity of 1.57 W/mK is sizably lower than the bulk value of 3.15 W/mK obtained previously within the same framework [56]. We investigated the origin of this effect by analyzing the solution of the Boltzmann transport equation within the single mode relaxation time approximation. The analysis of the phonon density of states and group velocities for the bulk and the nanowire supplemented by the calculated lifetimes of bulk phonons (from third order anharmonic force constants) allowed us to conclude that most of the reduction of the thermal conductivity is due to a reduction of the group velocities for frequencies above 50 $cm^{-1}$. The calculation of phonon dispersion relations for other NWs with diameters in the range 6.5-11.6 nm suggests that the thermal conductivity, albeit always lower than in the bulk, increases by decreasing the size of the NW. A similar effect was also found in crystalline silicon NWs [40, 41]. A lower lattice thermal conductivity with respect to the bulk would

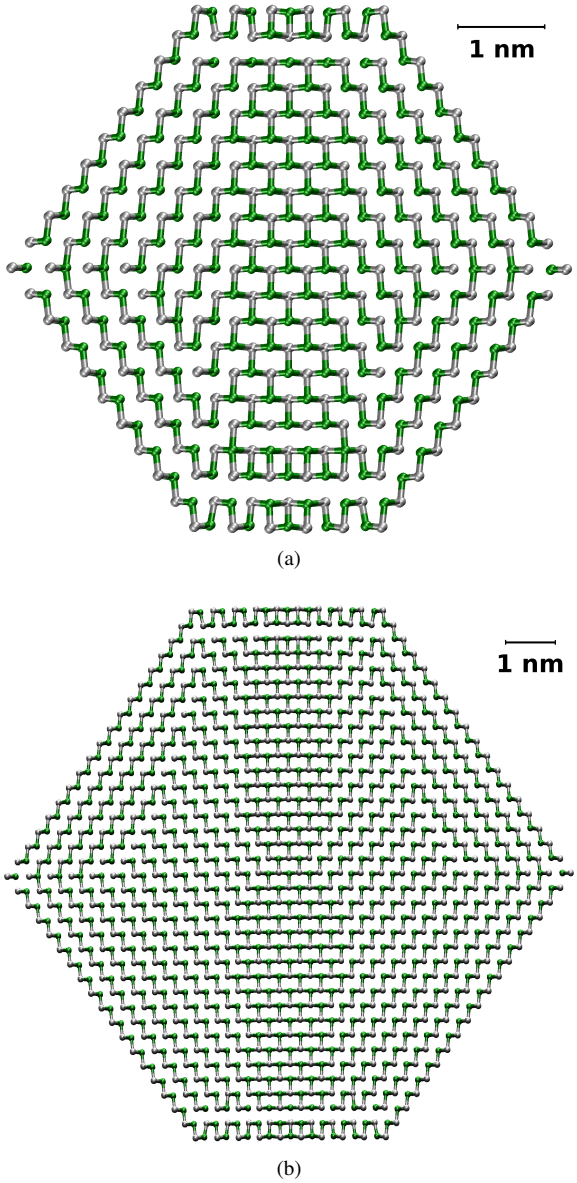


**Figure 7.** (Color online) Cross section of the GeTe NW with diameter of a) 6.5 nm and b) 11.6 nm.

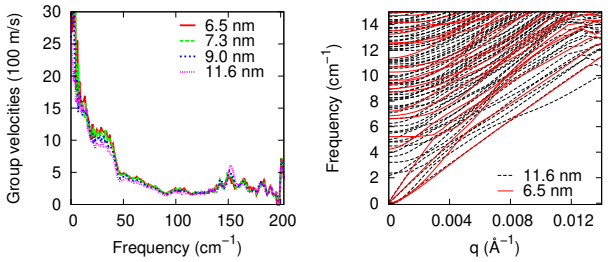


**Figure 8.** (Color online) Distribution of the group velocities for the four NWs with different diameters (left panel) and phonon dispersion relations along the growth direction of NWs with two representative diameters at low frequencies (right panel).

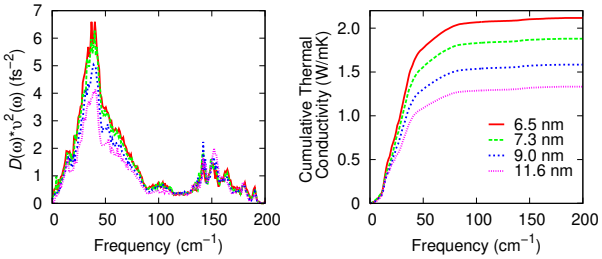


**Figure 9.** (Color online) (Left panel) $D(\omega) \cdot v_\alpha^2(\omega)$ of four NWs with diameters 6.5, 7.3, 9.0, and 11.6 nm. (Right panel) Cumulative lattice thermal conductivity obtained by plugging in (4) the function $D(\omega) \cdot v_\alpha^2(\omega)$ of the NWs and the phonon lifetimes $\tau(\omega)$ of the bulk (see text).

favor heat confinement along the NW axis which would also lead to a reduction in the programming current in memory applications.

## Acknowledgments

This work has been partially supported by the European Union Seventh Framework Programme FP7/2007-2013 under grant agreement No. 310339. We thankfully acknowledge the computational resources provided by Cineca (Casalecchio di Reno, Italy) through programs ISCRA and LISA.

[1] Fong S W, Neumann C M and Wong H S P 2017 *IEEE Trans. Electron Devices* **64** 4374
[2] Wuttig M and Yamada N 2007 *Nat. Mater.* **6** 824
[3] Pirovano A, Lacaita A L, Benvenuti A, Pellizzer F and Bez R 2004 *IEEE Trans. Electron. Dev.* **51**, 452
[4] Lacaita A L and Redaelli A 2013 *Microelectr. Eng.* **109** 351
[5] Lencer D, Salinga M and Wuttig M 2011 *Adv. Mat.* **23**, 2030
[6] Noé P, Vallée C, Hippert F, Fillot F, Raty J-Y 2018 *Semicond. Sci. Technol.* **33** 013002
[7] Zhang W, Mazzarello R, Wuttig M and Ma E 2019 *Nat. Rev. Mater.* **4** 150
[8] Ghezzi G E, Raty J-Y, Maitrejean S, Roule A, Elkaim E and Hippert F 2011 *Appl. Phys. Lett.* **99** 151906
[9] Rao F *et al.* 2017 *Science* **358** 1423
[10] Choe J 2017 TechInsights http://www.techinsights.com/about-techinsights/overview/blog/intel-3D-xpoint-memory-die-removed-from-intel-optane-pcm
[11] Lee S-H, Jung Y and Agarwal R 2007 *Nat. Nanotech.* **2** 626
[12] Piccione B, Agarwal R, Jung Y and Agarwal R 2013 *Phil. Mag.* **93** 2089
[13] Lee S-H, Jung Y and Agarwal R 2008 *Nano Lett.* **8** 3303
[14] Jung Y, Lee S-H, Ko D-K and Agarwal R 2006 *J. Am. Chem. Soc.* **128** 14026
[15] Longo M, Fallica R, Wiemer C, Salicio O, Fanciulli M, Rotunno E and Lazzarini L 2012 *Nano Lett.* **12** 1509-1515
[16] Jung C S *et al.* 2013 *Nano Lett.* **13** 543
[17] Lee S-H, Jung Y, Chung H, Jennings A T and Agarwal R 2008 *Physica E* **40** 2474
[18] Jung Y, Yang C-Y, Lee S-H and Agarwal R 2008 *Nano Lett.* **9** 2103
[19] Meister S, Peng H, McIlwrath K, Jarusch K, Zhang X F and Cui Y 2006 *Nano Lett.* **6** 1514
[20] Zuev Y M, Lee J S, Galloy C, Park H and Kim P 2010 *Nano Lett.* **10** 3037
[21] Rotunno E, Longo M, Wiemer C, Fallica R, Campi D, Bernasconi M, Lupini A R, Pennycook S J and Lazzarini L 2015 *Chemistry of Materials* **27** 4368
[22] Lee S-H, Ko D-K, Jung Y and Agarwal R 2006 *Appl. Phys. Lett.* **89** 223116
[23] Yu D, Wu J, Gu Q and Park H 2006 *J. Am. Chem. Soc.* **128** 8148
[24] Yim J W L, Xiang B and Wu J 2009 *J. Am. Chem. Soc.* **131** 14526
[25] Sun X, Yu B, Ng G and Meyyappan M 2007 *J. Phys. Chem. C* **111** 2421
[26] Longo M, Wiemer C, Salicio O, Fanciulli M, Lazzarini L and Rotunno E 2011 *J. Cryst. Growth* **315** 152
[27] Jennings A T, Jung Y, Engel J and Agarwal R 2009 *J. Phys. Chem. C* **113** 6898
[28] Chung H-S, Jung Y, Kim S C, Kim D-H, Oh K H and Agarwal R 2009 *Nano Lett.* **9** 2395
[29] Selmo S, Cecchi S, Cecchini R, Wiemer C, Fanciulli M, Rotunno E, Lazzarini L and Longo M 2016 *Phys. Status Solidi A* **213** 335
[30] Pirovano A, Lacaita A L, Pellizzer F, Kostylev S A, Benvenuti A and Bez R 2004 *IEEE Trans. Electron. Devices* **51** 714
[31] Ielmini D, Lacaita A L and Mantegazza D 2007 *IEEE Trans. Electron. Devices* **54**, 308
[32] Gabardi S, Caravati S, Sosso G C, Behler J and Bernasconi M 2015 *Phys. Rev. B* **2** 054201
[33] Mitra M, Jung Y, Gianola D S and Agarwal R 2010 *Appl. Phys. Lett.* **96** 222111
[34] Gabardi S, Baldi E, Bosoni E, Campi D, Caravati S, Sosso G C, Behler J and Bernasconi M 2017 *J. Phys. Chem. C* **121** 23827
[35] Sun X H, Yu B, Ng G, Nguyen T D and Meyyappan M 2006 *Appl. Phys. Lett.* **89** 233121
[36] Lepri S 2016 *Thermal Transport in Low Dimensions, from Statistical Physics to Nanoscale Heat Transfer* (Springer International Publishing, Switzerland)
[37] Zhang G and Zhang Y-W 2013 *Phys. Status Solidi RRL* **7** 754
[38] Li D *et al.* 2003 *Appl. Phys. Lett.* **83** 2934
[39] Mingo N 2003 *Phys. Rev. B* **68** 113308
Mingo N, Yang L, Li D and Majumdar A 2003 *Nano Lett.* **3** 1713
[40] Ponomareva I, Srivastava D, Menon M 2007 *Nano Lett.* **7** 1155
[41] Donadio D and Galli G 2009 *Phys. Rev. Lett.* **102** 195901
[42] Sosso G C, Miceli G, Caravati S, Behler J and Bernasconi M 2012 *Phys. Rev. B* **85** 174103
[43] Goldak J, Barrett C S, Innes D and Youdelis W 1966 *J. Chem. Phys.* **44** 3323
[44] Chattopadhyay T, Boucherle J and Von Schnering H 1987 *J. Phys. C* **20** 1431
[45] Fons P *et al.* 2010 *Phys. Rev. B* **82** 155209
[46] Matsunaga T, Fons P, Kolobov A V, Tominaga J and Yamada N 2011 *Appl. Phys. Lett.* **99** 231907
[47] Park S *et al.* 2015 *ACS Appl. Mater. Interfaces* **7** 21819
[48] Fallica R, Varesi E, Fumagalli L, Spadoni S and Longo M 2013 *Phys. Status Solidi RRL* **7** 1107
[49] Behler J and Parrinello M 2007 *Phys. Rev. Lett.* **98** 146401
Behler J 2011 *J. Chem. Phys.* **134** 074106
Behler J 2017 *Angew. Chemie* **56** 12828
[50] Perdew J P, Burke K and Ernzerhof M 1996 *Phys. Rev. Lett.* **7** 3865
[51] Mazzarello R, Caravati S, Angioletti-Uberti S, Bernasconi M and Parrinello M 2010 *Phys. Rev. Lett.* **104** 085503; erratum 2011 **107** 039902
[52] Caravati S, Bernasconi M, Kühne T D, Krack M and Parrinello M *Appl. Phys. Lett.* **91** 171906
[53] Akola J and Jones R O 2007 *Phys. Rev. B* **76** 235201
[54] Hegedüs J and Elliott S R 2008 *Nat. Mater.* **7** 399
[55] Sosso G C, Donadio D, Caravati S, Behler J and Bernasconi M 2012 *Phys. Rev. B* **86** 104301
[56] Campi D, Donadio D, Sosso G C, Behler J and Bernasconi M 2015 *J. Appl. Phys.* **117** 015304
[57] Sosso G C, Behler J and Bernasconi M 2012 *Phys. Status Solidi B* **249** 1880; erratum 2013 **250** 1453
[58] Sosso G C, Miceli G, Caravati S, Behler J and Bernasconi M 2013 *J. Phys. Chem. Lett.* **4** 4241
Sosso G C, Colombo J, Del Gado E, Behler J and Bernasconi M 2014 *J. Phys. Chem. B* **118** 13621
[59] Müller-Plathe F 1997 *J. Chem. Phys.* **106** 6082
[60] Behler J Institut für Physikalische Chemie, Universität Göttingen, Germany *RuNNer: A Neural Network Code for High-Dimensional Potential-Energy Surfaces*
[61] Smith W and Forester T R 1996 *J. Mol. Graph.* **14** 136
[62] Bevolo A J, Shanks H R and Eckels D E 1976 *Phys. Rev. B* **13** 3523
[63] Campi D, Paulatto L, Fugallo G, Mauri F and Bernasconi M 2017 *Phys. Rev. B* **95** 024311
[64] Baroni S, de Gironcoli S, Dal Corso A 2001 *Rev. Mod. Phys.* **73** 515
[65] Hajinazar S, Shao J and Kolmogorov A N 2017 *Phys. Rev. B* **95** 014114
[66] Fugallo G, Lazzeri M, Paulatto L and Mauri F 2013 *Phys. Rev. B* **88** 045430
[67] Lepri S, Livi R and Politi A 2003 *Phys Rep* **377** 1
[68] Lee V, Wu C H, Lou Z X, Lee W L and Chang C W 2017 *Phys. Rev. Lett.* **118** 135901
[69] Hsiao T K, Chang H K, Liou S C, Chu M W, Lee S C and Chang C W 2013 *Nat. Nanotech.* **8** 534
[70] Xu X, Pereira L F C, Wang Y, Wu J, Zhang K, Zhao X, Bae S, Tinh Bui C, Xie R, Thong J T L, Hong B H, Loh K P, Donadio D, Li B and Özyilmaz B 2014 *Nature Commun.* **5** 3689.
[71] Donadio D in "Thermal Transport in Low Dimensions: From Statistical Physics to Nanoscale Heat Transfer" Lepri S, Ed. 2016 Springer International Publishing, p. 275.